

# CLOSED-FORM COMPUTATION OF ELECTROMAGNETIC FIELDS IN INDUCTION MOTORS

Francisco de León\* and Sujit Purushothaman\*\*

## Abstract

A closed-form solution of the electromagnetic field equations for a three-phase squirrel-cage induction motor is presented. The analysis starts from the application of the Galilean transformation to Maxwell equations for moving media at constant speed. The induction motor is modelled as five concentric cylindrical layers representing the different construction components of the motor. By solving the Helmholtz and Laplace equations for conducting and non-conducting layers, we obtain a coupled set of Bessel and Euler equations that are solved analytically. The obtained formulas allow for the efficient calculation of important information for the designer regarding the electromagnetic fields, losses, force and torque. Parametric analyses are shown for illustration of the benefits of the closed form solution. The analytical expressions are validated against finite element simulations. Analytical expressions to compute the parameters of the equivalent circuit from the dimensions of the motor are also provided.

## Key Words

Induction motors, electromagnetic fields analysis, Galilean transformation, motor design

## 1. Introduction

The principles of the induction motor have been studied from the beginning of electromagnetics. Maxwell [1] and Hague [2], before the computer age, solved many problems analytically. However, it was not possible (at that time) to give numerical results from the formulas obtained without further simplifications. In the second half of the twentieth century, there have been important advances in the analytical solutions of electromagnetic field (EMF) problems related to induction motors. Smythe [3] compiled a large number of analytical solutions for fields in practical geometrical arrangements. Continuum electromechanics is the focus of the work by Melcher and Woodson [4], [5]. They also offer a clear description of the Galilean transformation

used in this paper to deal with rotation. Štafl [6] shows quantitative analyses of closed-form solutions of EMFs important for electrical machines. Slemon [7], [8] presents the practical application of the duality between magnetic and electric circuits. Perry [9] offers a modern view of low-frequency electromagnetic problems in machines using computers to obtain results for classical analytical formulations. Tegopoulos [10] discusses the analytical methods for determining the eddy current density and associated loss in linear conducting media at low frequencies.

Other classical and modern electrical machines books include: Chapman [11], Langsdorf [12], Liwschitz-Garik and Whipple [13], Alger [14], Krause *et al.* [15], Gross [16] and Levi [17] to name a few.

One of the earliest papers on power flow in induction machines based on field computations was by Alger [18]. In [19] and [20], an equivalent network for the induction machine based on EMF analysis is given.

Nowadays (year 2013), computation power has grown significantly and finite element analysis (FEA) on rotating machines is not only possible, but also commonly used to formulate mathematical models [21], [22] and verify designs. Even magneto-mechanical phenomena can be analysed using FEA [23]. 2D and 3D FEA can be performed when the cost of the machine justifies it. However, it is still not very convenient to include FEA in the loop of design programs since it is computationally intensive and setting up is time consuming. A small design modification may require setting up an entirely new case.

This paper presents a two-dimensional closed-form solution of the EMF problem in a three-phase induction motor. From the obtained expressions it is possible to draw interesting conclusions useful for the designer. One can perform, in a few seconds, parametric analyses of the terminal behaviour of the machine as the dimension and material properties are varied. For example, it is possible to compute: Joule effect losses; starting and name plate torques; magnetic flux density in all the regions and even the parameters of the equivalent circuit.

We acknowledge that the underlying theory (the solution of multi-layer travelling wave problems) presented in this paper is not new. Nevertheless, to the best of our knowledge, the complete analytical solution of the EMF

\* Department of Electrical and Computer Engineering, Polytechnic Institute of NYU, Brooklyn, NY; e-mail: fdeleon@poly.edu

\*\* FM Global Research, Norwood, MA; e-mail: p9sujit@yahoo.com

Recommended by Prof. A. Domijan

(DOI: 10.2316/Journal.203.2013.2.203-5079)

inside of an induction motor, representing the rotor as a solid conducting and rotating medium, has not been published before. Hague [2] and Levi [17] have published closed-form solutions of the EMF problem in an induction motor. However, in both cases the rotor windings are represented as current sheets. This precludes the possibility of studying the effect of dimensions and material properties of the rotor windings.

## 2. Electromagnetic Formulation

Figure 1 shows the geometrical arrangement considered for the EMF study in the induction machine. The induction motor is modelled using the following six concentric cylindrical regions:

1. Rotor iron core (ferromagnetic laminations)  $r = [0, a]$
2. Squirrel cage (combination of conducting material and ferromagnetic laminations)  $r = [a, b]$
3. Air gap  $r = [b, c]$
4. Stator iron core (ferromagnetic laminations)  $r = [c, d]$
5. Exterior (air)  $r = [d, \infty)$
6. Impressed current sheet  $r = c$

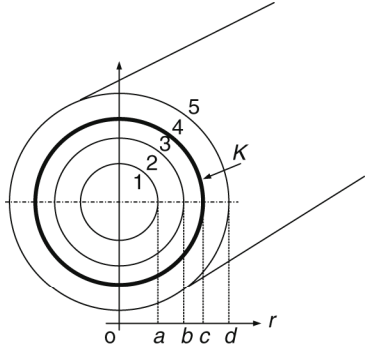


Figure 1. Regions for the EMF study in the induction motor.

Additional assumptions are as follows: linearity is considered, eddy currents in laminations are neglected, the axial length is considered infinity, the squirrel cage is substituted by a uniform conducting layer, and the stator windings are considered as an impressed current sheet of negligible thickness.

The analytical EMF study is performed considering that the motor is rotating at a constant angular speed  $\omega_m$ . The motor is excited by a three-phase balanced positive sequence and perfectly sinusoidal voltage source of electric frequency  $\omega_e$ . However because of the generality of the equations, any operating condition can be analysed.

The study starts from the Maxwell equations for the quasi-static conditions:

$$\nabla \times \bar{H} = \bar{J} \quad (1)$$

$$\nabla \times \bar{E} = -\frac{\partial \bar{B}}{\partial t} \quad (2)$$

Using the fact that  $\nabla \cdot \bar{B} = 0$ , we define  $\bar{A}$  (the magnetic vector potential) as:

$$\bar{B} = \nabla \times \bar{A} \quad (3)$$

The electromagnetic properties of the material are given by the following relations:

$$\bar{J} = \sigma \bar{E} \quad (4a)$$

$$\bar{B} = \mu \bar{H} \quad (4b)$$

Since the angular speed of the motor is considerably smaller than the speed of light we can obtain Maxwell equations for moving media using the Galilean transformation [3]–[5], [9], [10]. The resulting transformed Maxwell equations are:

$$\nabla \times \bar{H}' = \bar{J}' \quad (5)$$

$$\nabla \times (\bar{E} - \bar{\Omega} \times \bar{B}') = -\frac{\partial \bar{B}'}{\partial t} \quad (6)$$

Thus the relationships between the electromagnetic variables of the two systems, one standing and the other rotating (primed variables) at constant angular speed (vector  $\bar{\Omega}$ ) are:

$$\begin{aligned} \bar{E}' &= \bar{E} + \bar{\Omega} \times \bar{B}' \\ \bar{B}' &= \bar{B} \\ \bar{J}' &= \bar{J} \\ \bar{A}' &= \bar{A} \\ \bar{H}' &= \bar{H} \end{aligned} \quad (7)$$

For the regions where the conductivity may be considered zero (neglecting the eddy currents): rotor core, air gap, stator core and exterior, we need to solve Laplace's equation:

$$\nabla^2 A_z = 0 \quad (8)$$

For the squirrel cage (high conductivity material) we have:

$$(\nabla^2 + \gamma^2) \bar{A}_2 + \beta^2 \frac{\partial \bar{A}_2}{\partial \varphi} = 0 \quad (9)$$

$\gamma$  in (9) includes the effect of the known time variation  $e^{j\omega t}$  which is implicit in the all terms. The second term is due to the rotational speed. In cylindrical coordinates and considering the two remaining independent variables involved ( $r$  and  $\varphi$ ) (8) and (9) are reduced to:

$$\frac{\partial^2 A_z}{\partial r^2} + \frac{1}{r} \frac{\partial A_z}{\partial r} + \frac{1}{r^2} \frac{\partial^2 A_z}{\partial \varphi^2} = 0 \quad (10)$$

$$\begin{aligned} \frac{\partial^2 A'_{2z}}{\partial r^2} + \frac{1}{r} \frac{\partial A'_{2z}}{\partial r} + \frac{1}{r^2} \frac{\partial^2 A'_{2z}}{\partial \varphi^2} - \mu_2 \sigma_2 \omega_m \frac{\partial A'_{2z}}{\partial \varphi} \\ - j \mu_2 \sigma_2 \omega_e A'_{2z} = 0 \end{aligned} \quad (11)$$

We solve (10) and (11) using separation of variables. Consequently, the solutions are the product of two functions of only one variable  $A(r, \varphi) = R(r)\Phi(\varphi)$ . Because of

symmetry we know *a priori* that the variation as a function of  $\varphi$  should be  $e^{-jk\varphi}$ , where  $k$  is the number of pole pairs in the motor. The functions  $R(r)$  can be obtained by the solution of Euler and Bessel equations respectively for (10) and (11):

$$\frac{d^2 R(r)}{dr^2} + \frac{1}{r} \frac{dR(r)}{dr} - \frac{k^2}{r^2} R(r) = 0 \quad (12)$$

$$r^2 \frac{d^2 R_2(r)}{dr^2} + r \frac{dR_2(r)}{dr} - R_2(r)(k^2 + \alpha_1^2 r^2) = 0 \quad (13)$$

The parameter  $\alpha$  is a measurement of how much the EMF penetrates into the squirrel cage and is given by:

$$\alpha = \sqrt{j\mu_2\sigma_2(\omega_e - k\omega_m)} \quad (14)$$

$\alpha$  is closely related to the magnetic Reynolds number  $R_m$ , a quantity commonly used by motor designers to observe the effect of the speed in the penetration and distortion of the EMFs defined as  $R_m = \mu\sigma(\omega_e - k\omega_m)(b - a)^2$ .

Then, for the five regions of Fig. 1 we obtain the following set of solutions for the magnetic vector potential:

-Rotor iron core

$$A_{1z} = C_{12} r^k \sin(k\varphi) e^{j\omega_e t} \quad (15)$$

-Squirrel cage

$$A_{2z} = [C_{21} J_k(\alpha r) + C_{22} Y_k(\alpha r)] \sin(k\varphi) e^{j\omega_e t} \quad (16)$$

-Air gap

$$A_{3z} = [C_{31} r^{-k} + C_{32} r^k] \sin(k\varphi) e^{j\omega_e t} \quad (17)$$

-Stator iron core

$$A_{4z} = [C_{41} r^{-k} + C_{42} r^k] \sin(k\varphi) e^{j\omega_e t} \quad (18)$$

-Exterior

$$A_{5z} = C_{51} r^{-k} \sin(k\varphi) e^{j\omega_e t} \quad (19)$$

where  $J_k$  and  $Y_k$  are Bessel functions of the first kind and  $k$  order. Constants  $C_{ij}$  in (15) to (19) are evaluated from the boundary conditions. We have already omitted  $C_{11}$  and  $C_{52}$  from (15) and (19) because for  $r=0$  and  $r=\infty$  the field should vanish. For the remaining constants we use the following boundary conditions:

$$A_{zi} = A_{zi+1} - \frac{1}{\mu_i} \frac{\partial}{\partial r} (A_{zi}) + \frac{1}{\mu_{i+1}} \frac{\partial}{\partial r} (A_{zi+1}) = K \quad (20)$$

where  $K$  is the current sheet. In our case,  $K$  varies only with  $\varphi$  and runs in the axial direction.  $K(\varphi)$  represents an ideal balanced three-phase winding when given by [5], [7]:

$$K(\varphi) = \frac{N_{ds}}{2c} \sum_{h=1}^{\infty} \{I_{eff} \sin[kh\varphi] e^{j\omega_e ht}\} \quad (21)$$

where  $N_{ds}$  is the equivalent number of radial conductors of the stator winding. This current sheet is used as a representation of the travelling wave (rotating magnetic field). The spatial component can be expressed using Fourier series in order to consider deviations of the wave from the pure sinusoidal. For this study only the fundamental term ( $h=1$ ) is used. Higher values of  $h$  may be used to study higher harmonic fields.

Combining the two expressions in (20) with (14) to (18) we write a set of eight linear algebraic equations, where the unknowns are the constants  $C_{ij}$ . We have found the analytical solution in order to optimize the computer program. The resulting expressions are given in Appendix A.

As an alternate method, the eight equations can be solved numerically by writing them in the matrix form  $Ax=b$  ( $x=A^{-1}b$ ). Applying the boundary conditions given in (20) to (14) to (18) yields (in matrix form):

$$Mc = b \quad (22)$$

where,

$$c = [C_{12} \ C_{21} \ C_{22} \ C_{31} \ C_{32} \ C_{41} \ C_{42} \ C_{51}]^T \quad (23)$$

$$b = [0 \ 0 \ 0 \ 0 \ K(\varphi) \ 0 \ 0 \ 0]^T \quad (24)$$

$$M = \begin{pmatrix} m_{11} & m_{12} & m_{13} & 0 & 0 & 0 & 0 & 0 \\ m_{21} & m_{22} & m_{23} & 0 & 0 & 0 & 0 & 0 \\ 0 & m_{32} & m_{33} & m_{34} & m_{35} & 0 & 0 & 0 \\ 0 & m_{42} & m_{43} & m_{44} & m_{45} & 0 & 0 & 0 \\ 0 & 0 & 0 & m_{54} & m_{55} & m_{56} & m_{57} & 0 \\ 0 & 0 & 0 & m_{64} & m_{65} & m_{66} & m_{67} & 0 \\ 0 & 0 & 0 & 0 & 0 & m_{76} & m_{77} & m_{78} \\ 0 & 0 & 0 & 0 & 0 & m_{86} & m_{87} & m_{88} \end{pmatrix} \quad (25)$$

The coefficients of  $M$  are given in Appendix B.  $M$  is a band matrix. Therefore, the solution of (22) can be obtained very efficiently by Gauss reduction. The numerical solution is easy to compute and integrate in a design program.

Once the  $C_{ij}$ 's are known the vector potential  $\bar{A}$  is known in all regions. Therefore, analytical expressions for the magnetic flux density  $\bar{B}$  can be obtained using (3). This process yields:

$$\bar{B}_1 = C_{12} k r^{k-1} \cos(k\varphi) e^{j\omega_e t} \hat{e}_r - C_{12} k r^{k-1} \sin(k\varphi) e^{j\omega_e t} \hat{e}_\varphi \quad (26)$$

$$\begin{aligned} \bar{B}_2 = & k r^{-1} [C_{21} J_k(\alpha r) + C_{22} Y_k(\alpha r)] \cos(k\varphi) e^{j\omega_e t} \hat{e}_r \\ & + 0.5\alpha \sin(k\varphi) [-C_{21} (J_{k-1}(\alpha r) + J_{k+1}(\alpha r)) \\ & + C_{22} (Y_{k+1}(\alpha r) - Y_{k-1}(\alpha r))] e^{j\omega_e t} \hat{e}_\varphi \end{aligned} \quad (27)$$

$$\begin{aligned} \overline{B}_3 = & kr^{-k-1}(C_{31} + C_{32}r^{2k}) \cos(k\varphi)e^{j\omega_e t}\hat{e}_r \\ & + kr^{-k-1}(C_{31} - C_{32}r^{2k}) \sin(k\varphi)e^{j\omega_e t}\hat{e}_\varphi \end{aligned} \quad (28)$$

$$\begin{aligned} \overline{B}_4 = & kr^{-k-1}(C_{41} + C_{42}r^{2k}) \cos(k\varphi)e^{j\omega_e t}\hat{e}_r \\ & + kr^{-k-1}(C_{41} - C_{42}r^{2k}) \sin(k\varphi)e^{j\omega_e t}\hat{e}_\varphi \end{aligned} \quad (29)$$

$$\begin{aligned} \overline{B}_5 = & C_{51}kr^{-k-1} \cos(k\varphi)e^{j\omega_e t}\hat{e}_r \\ & + C_{51}kr^{-k-1} \sin(k\varphi)e^{j\omega_e t}\hat{e}_\varphi \end{aligned} \quad (30)$$

Using (4b) we can compute the magnetic field strength  $\overline{H}$ , and the current density  $\overline{J}$  is calculated from (5) as:

$$J_{2z} = \frac{\alpha^2}{\mu_2} [C_{21}J_k(\alpha r) + C_{22}Y_k(\alpha r)] \sin(k\varphi)e^{j\omega_e t} \quad (31)$$

Note that  $\overline{J}$  has only in the  $z$  component and only exists in region 2, which is the conductive layer representing the squirrel cage. The consumed apparent power of the motor is calculated from the Poynting vector as:

$$S = - \int_S \overline{\Pi} \cdot d\overline{S} = \frac{1}{2} \int_S (\overline{E} \times \overline{H}^*) \cdot d\overline{S} \quad (32)$$

The real part of (32) can be used to compute the losses and torque, while the imaginary part gives the leakage and magnetizing inductances.

The force density is given by the following expression:

$$\overline{F} = \frac{1}{2} \overline{J} \times \overline{B}^* \quad (33)$$

This force can be divided into the following two directional components as:

$$\overline{F} = F_r \hat{e}_r + F_\varphi \hat{e}_\varphi \quad (34)$$

Developing the  $\varphi$  component of (34) as  $F_\varphi = J_z B_r$  and substituting (27) and (31), we get:

$$F_\varphi = \frac{k}{2\mu_2 r} |\alpha [C_{21}J_k(\alpha r) + C_{22}Y_k(\alpha r)]|^2 \sin(2k\varphi) \quad (35)$$

The torque  $T$  can be obtained from:

$$T = \int_V r F_\varphi dV \quad (36)$$

which can be written as:

$$\begin{aligned} T = & 4 \frac{k}{\mu_2} \int_{r=a}^b \int_{\varphi=0}^{\pi/4} \int_{z=0}^l |\alpha [C_{21}J_k(\alpha r) + C_{22}Y_k(\alpha r)]|^2 \\ & \times \sin(2k\varphi) r dr d\varphi dz \end{aligned} \quad (37)$$

The integrals in (37) can be evaluated numerically or analytically using expressions from [24]; the former was done in this paper.

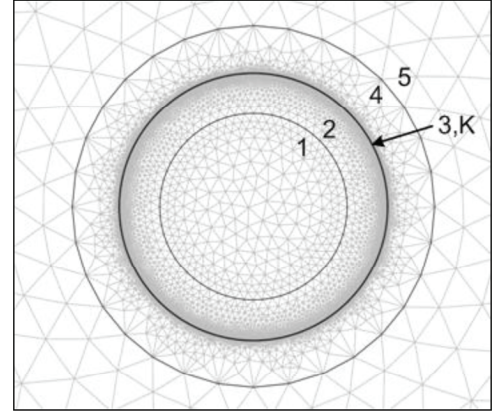


Figure 2. FEM mesh for the five regions.

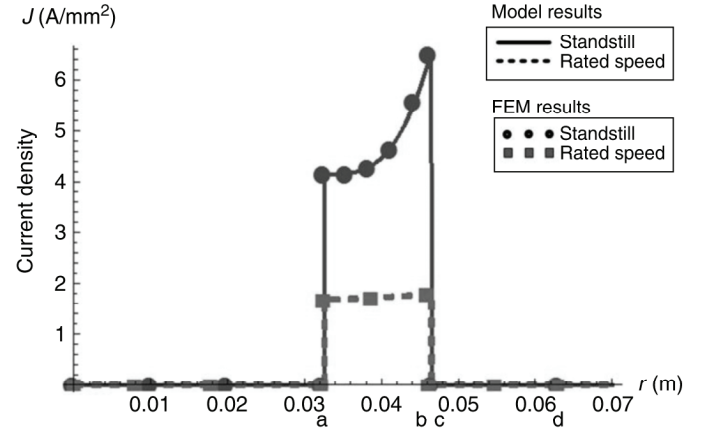


Figure 3. Comparison of the analytical solution and FEM results for current density in the squirrel cage at standstill and rated speed (two poles).

### 3. Accuracy Comparison against Finite Elements

To validate the obtained closed-form solution, the same motor geometry was simulated using a commercial finite element method (FEM) program; Fig. 2 presents the utilized mesh. Although with FEM one can solve a more realistic geometrical configuration [25], FEM is used here for comparison purposes; therefore, we use the same arrangement as Fig. 1. Layer 3, representing the air gap, is not visible in the figure when drawn to scale.

Figure 3 plots the variation of current density ( $J$ ) computed with FEM and the model presented in this paper (31) for standstill (high slip) and rated speed (low slip). Both solutions are in good agreement; therefore, validating the presented method. Since the frequency of induced currents in the rotor is slip times the power frequency, large eddy currents at power frequency are induced at standstill in the squirrel cage. At power frequency, most of the current is concentrated at the surface due to small field penetration depth caused by skin effect. At rated speed (low slip), when the penetration depth is large, the induced currents are almost uniformly distributed.

Figure 4a and 4b shows the radial and  $\varphi$  components of magnetic flux density at low and high slip (rated and

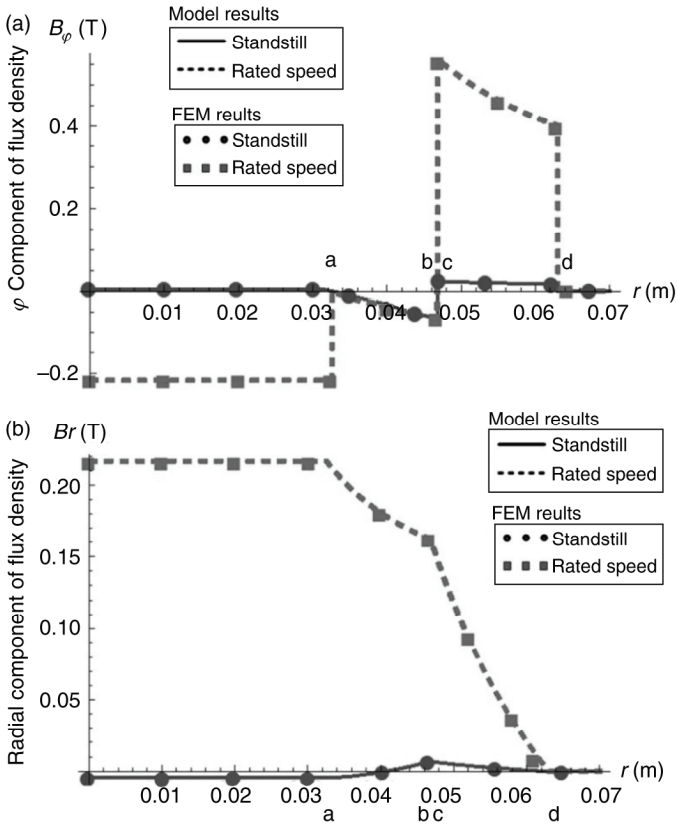


Figure 4. (a) Comparison of the analytical solution and FEM results for the  $\varphi$  component of the magnetic flux density at standstill and rated speed (two poles). Plotted at  $\varphi = 90$ . (b) Comparison of the analytical solution and FEM results for radial component of magnetic flux density at standstill and rated speed (two poles). Plotted at  $\varphi = 0$ .

standstill speed). Results from the proposed model are compared against FEM. At high slip (standstill), leakage flux (armature reaction) is significant, while at low slip (rated speed) magnetizing flux dominates. Hence the magnitude of the flux density at rated speed is substantially larger than at standstill.

Figures 5 and 6 present the streamline plots for the magnetic flux density at standstill and rated speed, respectively. These plots corroborate the results from Figs. 3 and 4. At low slip, the large field penetration depth leads to more flux lines penetrating the squirrel cage into the iron core. Alternately, at high slip, the small penetration depth results in less flux lines penetrating into the core and more flux lines concentrated in the air gap.

#### 4. Parametric Analyses

A series of parametric analyses are performed in this section to illustrate the benefits of our solution. With the analytical equations we can produce, in seconds, curves revealing the tendencies of terminal parameters as we vary physical dimensions, material properties or operating conditions.

In Fig. 7 we present the power density (Poynting vector) for standing still and rated speed conditions. We can see that the power density reaches about thrice as large

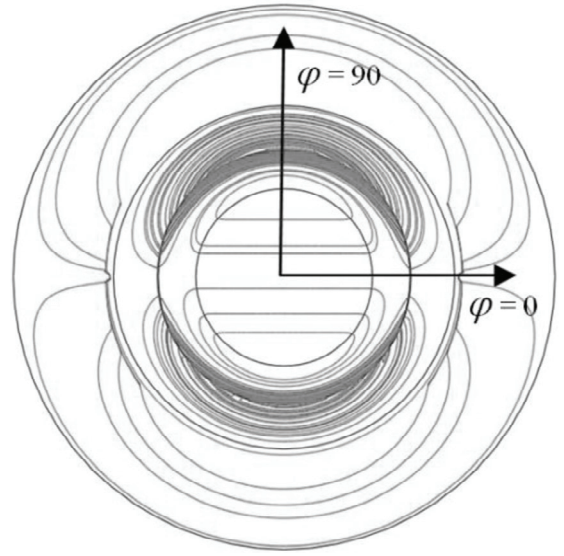


Figure 5. Streamline plot for magnetic flux (leakage) density for standing conditions.

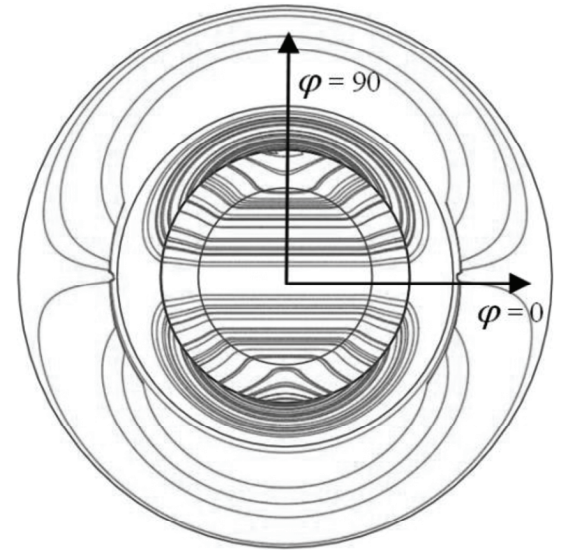


Figure 6. Streamline plot for magnetic flux (magnetizing) density for rated speed.

for standing conditions as for name plate speed. The power density distribution gives important information to the designer on where and when the force, torque and losses are generated. We observed that for  $\omega_m = 0$ , the power density follows a non-uniform distribution with an increasing slope (w.r.t.  $r$ ), meanwhile for  $\omega_m = \text{rated}$  the slope decreases with  $r$ , but the power, torque and losses are still being produced mainly close to the rotor surface. Equation (37) can be evaluated at various speeds to obtain torque-speed characteristics. Figure 8a shows the  $T$ - $\omega$  characteristic for the induction machine modelled in the paper and also depicts the effect of increasing rotor resistance on the torque-speed characteristics. It is observed that while the maximum torque (breakdown torque) remains the same, the slip at which maximum torque occurs (critical slip) is higher with increasing resistance.

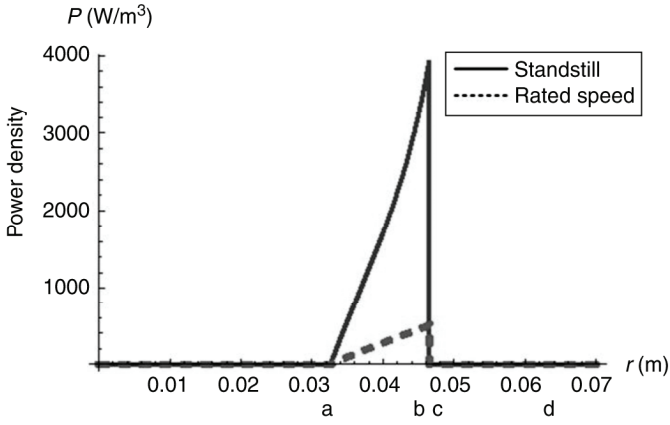


Figure 7. Power density (Poynting vector) at standstill and rated speed (two poles).

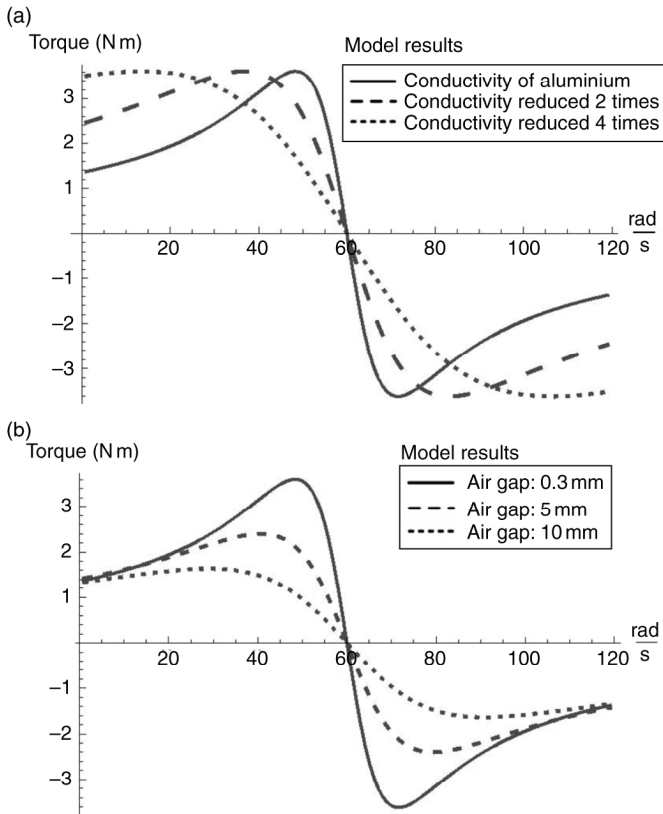


Figure 8. (a) Effect of increasing resistivity of squirrel cage (rotor resistance  $R_2$ ) on torque speed characteristics for the modelled machine. (b) Effect of increasing air gap (rotor leakage reactance  $X_2$ ) on torque speed characteristics for the modelled machine.

Figure 8b shows the variation in the torque-speed curves when varying the air gap length computed with (37). Increasing the air gap length increases the reluctance and consequently increasing the leakage reactance. The breakdown torque of an induction machine is inversely proportional to the leakage reactance. Hence, Fig. 8a and 8b is in accordance with the classical theory of induction machines. Magnetizing reactance is an important factor to be considered while designing an induction machine. Increasing the air gap requires more magnetizing volt-ampere

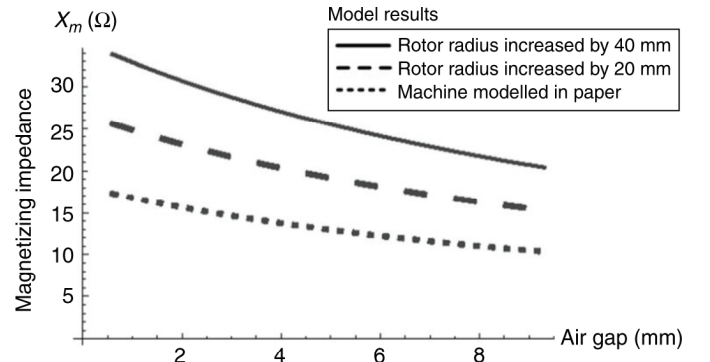


Figure 9. Variation of magnetizing reactance with increase in air gap for increasing dimensions of rotor and stator size.

from the source, effectively reducing the magnetizing reactance. Figure 9 shows this variation with air gap length for various rotor and stator sizes.

## 5. Equivalent Circuit Parameters

The equivalent circuit parameters have been extensively used by designers and analysts to study the performance characteristics of induction machines. This section creates a link between the analytical model presented in this paper and the equivalent circuit for induction machines.

The leakage and magnetizing reactances are found by performing the locked rotor and no-load test, respectively. The leakage reactance can be evaluated from the leakage field which is the  $\varphi$  component of the magnetic field in the air gap at standstill. Similarly, the magnetizing reactance can be found using the magnetic energy in all the regions at synchronous speed. This is equivalent to performing the tests on the machine.

For  $\omega_m = 0$ :

$$\frac{1}{2}L_2I^2 = \int_{V_3} \frac{1}{2}\mu_3 H_{3\varphi}^2 dV \quad (38)$$

For  $\omega_m = k\omega_e$ :

$$\frac{1}{2}L_mI^2 = \sum_{i=1}^5 \int_{V_i} \frac{1}{2}\mu_i H_i^2 dV \quad (39)$$

where

$L_2$  = leakage reactance

$L_m$  = magnetizing reactance

$H_i$  = magnetic field  $H$  in  $i$ th region

$I$  = applied excitation (current sheet  $K_\varphi$ )

with [7]:

$$K_\varphi = \frac{3N_{ds}}{4c}I \quad (40)$$

Analogous to the method followed to calculate the rotor resistance from the blocked rotor test, the rotor resistance  $R_2$  is found from the  $\varphi$  component of the Poynting vector at standstill as:

$$I^2 R_2 = \text{Re}(S_\varphi) \quad (41)$$

The loss (heat) producing component of rotor resistance  $R_{2loss}$  can be found from the radial component of Poynting vector as:

$$I^2 R_{2loss} = \text{Re}(S_r) \quad (42)$$

where from (32):

$$\bar{S} = S_r \hat{e}_r + S_\varphi \hat{e}_\varphi \quad (43)$$

$S_r$  is evaluated over the surface of the squirrel cage, whereas  $S_\varphi$  is evaluated over the radial cross section of the squirrel cage. It must be noted that the radial component is dissipated in the rotor while the  $\varphi$  component is responsible for producing the torque in the squirrel cage.

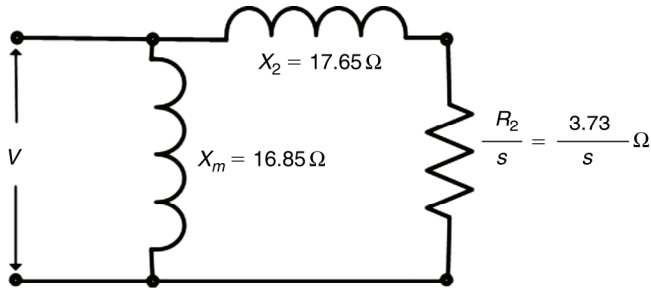


Figure 10. Traditional equivalent electrical circuit for modelled motor.

The induction machine equivalent circuit with parameters calculated as above is given in Fig. 10. It must be noted that the stator resistance is not included. Figure 11 shows the torque-speed characteristics as obtained from the model, FEM, equivalent circuit obtained from the model (no stator) and the complete equivalent circuit. It is observed that results from the model of this paper and FEM are a perfect match, while the equivalent circuit gives small differences. The eddy current and hysteresis losses in the core can be analysed by the model presented in [26].

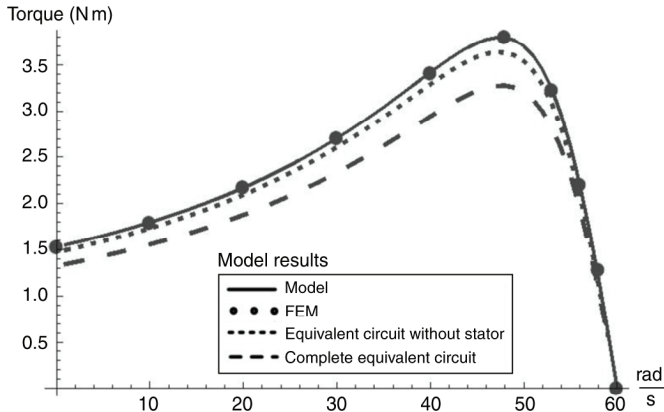


Figure 11. Comparison of torque-speed characteristics obtained from model, FEM and equivalent circuit without stator and complete equivalent circuit.

## 6. Conclusions

A closed-form solution for the EMFs inside of a three-phase squirrel-cage induction motor has been presented. The analysis is based on the Galilean transformation of Maxwell equations for moving media at constant speed.

The obtained analytical expressions have been compared against finite elements yielding virtually the same results for a cylindrical geometry.

A large amount of information can be obtained from the model of this paper in addition to the distribution of the EMFs inside the machine. For example: the starting and rated speed torques; losses; the effect of changing the number of poles, increasing air gap, changing the materials used in the machine and changing the dimensions of each region to name a few.

The paper has established a link between the equivalent electrical circuit parameters and the physical dimensions and material properties of the machine. The information obtained from a study of this nature is directly applicable to the designer. The formulas are a much faster alternative to the FEM for computing the EMF in induction motors.

## 7. Future Work

We intend to include, in a sequel paper, the stator modelled as a uniform region with adequate conductivity and permeability by the method of Freeman [27]. This should help in obtaining the performance parameters of the stator as well. Currently, we are investigating the effects of teeth and slots in both stator and rotor to establish the validity range of Carter's coefficient [28].

The formulas of this paper can be utilized for the design of induction machines. We plan to use them to design the induction machine damping unit (IMDU) used in [29] to damp sub-synchronous resonance. The obtained solution can also be applied to model doubly-fed induction machines currently very popular for wind-turbine applications.

## Appendix A

### Constants for (14) to (18)

$$\begin{aligned} C_{12} &= \frac{a^{1-k} \alpha \mu_1 \mu_2 R_{sra} G_{c1}}{Q_{c1}} \\ C_{21} &= \frac{\mu_2 G_{c1} (\alpha a \mu_1 Y_{ra} - 2k \mu_2 Y_{sa})}{F_{s4} + F_{s5} (\mu_1 - \mu_3)} \\ C_{22} &= \frac{\mu_2 G_{c1} (-\alpha a \mu_1 J_{ra} + 2k \mu_2 J_{sa})}{Q_{c1}} \\ C_{31} &= \frac{b^{-k} G_{c1} T_{j1}}{4k (F_{s4} + F_{s5} (\mu_1 - \mu_3))} \\ C_{32} &= \frac{c^{-k} N_{ds} V_i F_{s3} \mu_1 \mu_3 T_{j2}}{4Q_{c1} k} \\ C_{41} &= -\frac{d^{2k} G_{c2} (\mu_1 + \mu_3)}{4Q_{c1} k} \end{aligned} \quad (44)$$

$$C_{42} = \frac{G_{c2}(\mu_1 - \mu_3)}{4Q_{c1}k}$$

$$C_{51} = -\frac{d^{2k}G_{c2}\mu_3}{2Q_{c1}k}$$

where:

$$G_{c1} = b^k c^k F_{s3} \mu_1 \mu_3 N_{ds} V_i$$

$$G_{c2} = c^k (T_{j1} + T_{j2}) \mu_1 \mu_3 N_{ds} V_i \quad (45)$$

$$Q_{c1} = c^{2k}(\mu_1 - \mu_3)P_{m1} + d^{2k}(\mu_1 + \mu_3)P_{m2} \quad (46)$$

$$F_{s1} = c^{2k}(\mu_1 - \mu_3)^2 - d^{2k}(\mu_1 + \mu_3)^2$$

$$F_{s3} = c^{2k}(\mu_1 - \mu_3) - d^{2k}(\mu_1 + \mu_3)$$

$$F_{s4} = c^{2k}(2T_{j3}k\mu_2(\mu_1 + \mu_3) + \alpha a \mu_1(-F_{s1}S_{m2} + b^{2k}S_{m1}(\mu_1^2 - \mu_3^2)))$$

$$F_{s5} = 2c^{4k}S_{m3}k\mu_2(\mu_1 - \mu_3) - d^{2k}T_{j1}(\mu_1 + \mu_3) \quad (47)$$

$$P_{m2} = T_{j1}(\mu_3 - \mu_1) + T_{j2}(\mu_3 + \mu_1)$$

$$P_{m1} = T_{j2}(\mu_3 - \mu_1) + T_{j1}(\mu_3 + \mu_1) \quad (48)$$

$$T_{j1} = b^{2k}(\alpha a S_{m1} \mu_1 - 2S_{m4} k \mu_2)$$

$$T_{j2} = c^{2k}(\alpha a S_{m2} \mu_1 - 2S_{m3} k \mu_2)$$

$$T_{j3} = -b^{2k}S_{m4}(\mu_1 - \mu_3) - d^{2k}S_{m3}(\mu_1 + \mu_3) \quad (49)$$

$$S_{m4} = 2R_{ss}k\mu_2 + \alpha b R_{sr} \mu_3$$

$$S_{m3} = 2R_{ss}k\mu_2 - \alpha b R_{sr} \mu_3$$

$$S_{m2} = 2R_{rs}k\mu_2 + \alpha b R_{rr} \mu_3$$

$$S_{m1} = 2R_{rs}k\mu_2 - \alpha b R_{rr} \mu_3 \quad (50)$$

$$R_{sra} = J_{sa}Y_{ra} - J_{ra}Y_{sa}$$

$$R_{rs} = J_{sb}Y_{ra} - J_{ra}Y_{sb}$$

$$R_{ss} = J_{sb}Y_{sa} - J_{sa}Y_{sb}$$

$$R_{sr} = J_{sa}Y_{rb} - J_{rb}Y_{sa}$$

$$R_{rr} = J_{rb}Y_{ra} - J_{ra}Y_{rb} \quad (51)$$

$$V_i = [i_a + i_b + i_c] + [i_a + i_b e^{j\frac{2\pi}{3}} + i_c e^{j\frac{4\pi}{3}}] \quad (52)$$

$$J_{sb} = J_k(\alpha b)$$

$$J_{sa} = J_k(\alpha a)$$

$$Y_{sa} = Y_k(\alpha a)$$

$$Y_{sb} = Y_k(\alpha b)$$

$$J_{ra} = J_{k-1}(\alpha a) - J_{k+1}(\alpha a)$$

$$J_{rb} = J_{k-1}(\alpha b) - J_{k+1}(\alpha b)$$

$$Y_{ra} = Y_{k-1}(\alpha a) - Y_{k+1}(\alpha a)$$

$$Y_{rb} = Y_{k-1}(\alpha b) - Y_{k+1}(\alpha b) \quad (53)$$

## Appendix B

### Elements of Matrix M (25)

$$m_{11} = \frac{-k}{\mu_1} a^{k-1}, m_{12} = \frac{\alpha J_{rb}}{2\mu_2}, m_{13} = \frac{\alpha Y_{rb}}{2\mu_2}$$

$$m_{21} = ka^{k-1}, m_{22} = \frac{kJ_{sa}}{a}, m_{23} = \frac{kY_{sa}}{a}$$

$$m_{32} = -\frac{\alpha J_{rb}}{2\mu_2}, m_{33} = -\frac{\alpha Y_{rb}}{2\mu_2}$$

$$m_{34} = -\frac{k}{\mu_3} b^{-k-1}, m_{35} = \frac{k}{\mu_3} b^{k-1}$$

$$m_{42} = \frac{kJ_{sb}}{b}, m_{43} = \frac{kY_{sb}}{b} \quad (54)$$

$$m_{44} = -kb^{-k-1}, m_{45} = -kb^{k-1}$$

$$m_{54} = \frac{k}{\mu_3} c^{-k-1}, m_{55} = -\frac{k}{\mu_3} c^{k-1}$$

$$m_{56} = -\frac{k}{\mu_1} c^{-k-1}, m_{57} = \frac{k}{\mu_1} c^{k-1}$$

$$m_{64} = kc^{-k-1}, m_{65} = kc^{k-1}$$

$$m_{66} = -kc^{-k-1}, m_{67} = -kc^{k-1}$$

$$m_{76} = \frac{k}{\mu_1} d^{-k-1}, m_{77} = -\frac{k}{\mu_1} d^{k-1}, m_{78} = -\frac{k}{\mu_3} d^{-k-1}$$

$$m_{86} = kd^{-k-1}, m_{87} = kd^{k-1}, m_{88} = -kd^{-k-1}$$

## Appendix C

### Specification of Motor for Analysis

Manufacturer: General Electric (Excel)

Model: 6K48GB

Rated power: 1 HP

No of poles: 4/2

Line (stator) voltage: 220/440 V

Current: 3.4/1.7 A

Rated speed: 1725 rpm

Dimensions:

$a = 0.0326$  m;

$b = 0.0465$  m;

$c = 0.0468$  m;

$d = 0.0630$  m;

Properties:

$\mu_1 = \mu_4 = 1500\mu_0$ ;

$\mu_2 = \mu_3 = \mu_5 = \mu_0$ ;

$\sigma_2 = 1.8 \times 10^7$  S/m;

$k = 1$ ;

$N_{sd} = 86$ .

### Acknowledgements

The authors would like to recognize the contribution of Enrique Bernal-Luna who started this work. It is very unfortunate that he could not see the final product. The authors would also like to thank Dr. Layth Qaseer for his careful review of the mathematical derivations and his input clearing the equations from typographical errors.

## References

- [1] J.C. Maxwell, *A treatise on electricity and magnetism* (New York, NY: Dover Publications, 1954).
- [2] B. Hague, *Electromagnetic problems in electrical engineering* (Oxford: University Press, 1929).
- [3] W.R. Smythe, *Static and dynamic electricity* (New York, NY: McGraw-Hill, 1950).
- [4] J.R. Melcher, *Continuum electromechanics* (Cambridge, MA: M.I.T. Press, 1981).
- [5] H.H. Woodson and J.R. Melcher, *Electromechanical dynamics* (New York, NY: John Wiley & Sons, 1968).
- [6] M. Štafl, *Electrodynamics of electrical machines* (Czechoslovakia: Prague, Academia, 1967).
- [7] G.R. Slemon, *Electric machines and drives* (Reading, MA: Addison-Wesley Publishing Company Inc., 1992).
- [8] G.R. Slemon, Equivalent circuits for transformers and machines, including non-linear effects, *IEE Proceedings*, 100(4), 1953, 129–143.
- [9] M.P. Perry, *Low frequency electromagnetic design* (New York, NY: Marcel Decker Inc., 1985).
- [10] J.A. Tegopoulos, *Eddy currents in linear conducting media* (New York, NY: Elsevier Science Publishers, 1985).
- [11] S.J. Chapman, *Electric machinery fundamentals* (New York, NY: Mc-Graw Hill, 1998).
- [12] A. Langsdorf, *Theory of alternating current machinery* (New York, NY: Mc-Graw Hill Education, 1985).
- [13] M. Liwschitz-Garik and C.C. Whipple, *Electric machinery, A-C machines 2* (Princeton, NJ: D. Van Nostrand Company, 1946).
- [14] P.L. Alger, *Induction machines; their behavior and uses* (Gordon and Breach Science Publishers Inc., 1970).
- [15] P.C. Krause, O. Wasynczuk, and S.D. Sudhoff, *Analysis of electric machinery and drive systems*, 2nd ed. (New York: Wiley-IEEE, 2002).
- [16] C.A. Gross, *Electric machines* (Boca Raton, Florida: CRC Press; Taylor & Francis Group, LLC, 2007).
- [17] E. Levi, *Polyphase motors: a direct approach to their design* (John Wiley & Sons, 1984).
- [18] P.L. Alger and W.R. Oney, Torque–energy relations in induction machines, *AIEE Transactions on Power Apparatus and Systems*, 73(1), 1954, 259–264.
- [19] A.D. Napoli, Induction machine equivalent network parameters computation from electrical and magnetic fields analysis, *IEEE Transactions on Magnetics*, 15(6), 1979, 1470–1472.
- [20] G. Vinsard and B. Laporte, A new formulation for induction machine computation, *IEEE Transactions on Magnetics*, 30(5), 1994, 3693–3696.
- [21] K. Yamazaki, Comparison of induction motor characteristics calculated from electromagnetic field and equivalent circuit determined by 3D FEM, *IEEE Transactions on Magnetics*, 36(4), 2000, 1881–1885.
- [22] M. Mirzaei, M. Mirsalim, and S.E. Abdollahi, Analytical modeling of axial air gap solid rotor induction machines using a quasi-three-dimensional method, *IEEE Transactions on Magnetics*, 43(7), 2007, 3237–3242.
- [23] K. Fonteyn, A. Belahcen, R. Kouhia, P. Rasilo, and A. Arkkio, FEM for directly coupled magneto-mechanical phenomena in electrical machines, *IEEE Transactions on Magnetics*, 46(8), 2010, 2923–2926.
- [24] M. Abramowitz and I.A. Stegun, *Handbook of mathematical functions with formulas, graphs, and mathematical tables* (New York: Dover Publications, 1972).
- [25] S. Salon, M.V.K. Chari, K. Sivasubramaniam, O. Kwon, and J. Selvaggi, Computational electromagnetics and the search for quiet motors, *IEEE Transactions on Magnetics*, 45(3), 2009, 1694–1699.
- [26] J. Pippuri and A. Arkkio, Time-harmonic induction-machine model including hysteresis and eddy currents in steel laminations, *IEEE Transactions on Magnetics*, 45(7), 2009, 2981–2989.
- [27] E.M. Freeman, Travelling waves in induction machines: input impedance and equivalent circuits, *Proc. Institution of Electrical Engineers*, 115, 1968, 1772–1776.
- [28] F.W. Carter, The magnetic field of the dynamo-electric machine, *Journal IEE.*, 64, 1926, 1115–1138.
- [29] S. Purushothaman and F. de Leon, Eliminating sub-synchronous oscillations with an induction machine damping unit (IMDU), *IEEE Transactions on Power Systems*, 26(1), 2011, 225–232.

## Biographies



*Francisco de León* received the B.Sc. and the M.Sc. (Hons.) degrees in electrical engineering from the National Polytechnic Institute, Mexico City, Mexico, in 1983 and 1986, respectively, and the Ph.D. degree in electrical engineering from the University of Toronto, Toronto, ON, Canada, in 1992. He has held several academic positions in Mexico and has worked for the Canadian Electric

Industry. Currently, he is an associate professor at the Polytechnic Institute of NYU, Brooklyn, NY. His research interests include the analysis of power definitions under non-sinusoidal conditions, the transient and steady-state analyses of power systems, the thermal rating of cables and transformers, and the calculation of electromagnetic fields applied to machine design and modelling.



*Sujit Purushothaman* received his B.E. degree in electrical engineering from Mumbai University (Sardar Patel College of Engineering), Mumbai, India in 2005. His work experience includes testing and development of medium voltage switchgear for Siemens in Mumbai, India. He received his Master's and his Ph.D. degrees in electrical engineering from Polytechnic Institute of NYU in 2009

and 2011, respectively. He is currently a research engineer at FM Global Research in Norwood, MA. His research interests include power system transients, damping of sub-synchronous resonance, machine design and modelling, and thermal modelling of electrical devices.